Pis'ma v ZhETF, vol. 85, iss. 10, pp. 589 – 593

Terrestrial gamma-ray flashes and neutron pulses from direct simulations of gigantic upward atmospheric discharge

L. P. Babich[1)], *A. Yu. Kudryavtsev*[1)], *M. L. Kudryavtseva, I. M. Kutsyk*

Russian Federal Nuclear Center – VNIIEF, Sarov, Russia

Submitted 16 February 2007

Resubmitted 26 March 2007

Gamma-ray pulses are calculated from 2D numerical simulations of upward atmospheric discharge in selfconsistent electric field using multi-group approach to the kinetics of relativistic runaway electrons. Calculated numbers and spectra of γ-rays are consistent with the data on terrestrial γ-ray flashes observed aboard spacecrafts. The calculated runaway electron flux is concentrated mainly within the domain of the Blue Jet fluorescence. This proves that exactly this domain is a source of the γ-ray flashes. One γ-ray flash generates $\sim 10^{14}-10^{15}$ photonuclear neutrons.

PACS: 94.10.–s, 94.20.–y

High-energy phenomena connected with thunderstorm activity have been firmly established during last decades. Either ensue from the electron acceleration to high energies in atmosphere by thunderstorm electric fields as predicted by Wilson [1] and termed "electron runaway" [2].

Strong increase of x-rays inside thunderclouds above the fine weather background [3, 4] is one of these phenomena. Terrestrial γ-ray flashes (TGFs) observed aboard artificial satellites of the Earth BETSI [5] and RHESSI [6] is the second high-energy phenomenon. TGFs are acknowledged to be a consequence of upward atmospheric discharges (UADs) developing due to the breakdown in the atmosphere driven by relativistic runaway electrons (REs) [7].

Amplification of neutron flux in the troposphere during thunderstorms over the fine-weather background [8–10] is the third high-energy phenomenon: terrestrial neutron flashes (TNFs). Following to Fleisher [11] the neutron flux enhancement was interpreted in [8 – 10] as a result of nuclear reaction ^{2}H(^{2}H,n)^{3}He in lightning channel. The nuclear synthesis is absolutely impossible under physical conditions inherent for the lightning channel, and the neutrons could be generated by photonuclear reactions (γ, n) accompanying TGFs [12]. In the framework of the UAD analytical model with allowing for the geomagnetic field [13] the (γ, n)-yield was estimated as $\sim 10^{15}$ neutrons per UAD [12].

The theory of UAD is being developed basing on the classical mechanism of breakdown by low-energy electrons in strong electric field produced high above thundercloud owing to the lightning discharge in the troposphere (see, for instance, [14 – 20]). In the framework of this approach the high-altitude optical phenomena are described adequately, but difficulties appear with TGFs and TNFs. So, electron energizing up to 2–8 keV Moss et al. predicted in the field ahead of the streamer front [20] is too small to account for the TGFs and TNFs. To bypass this difficulty Moss et al. carried out evaluations to justify a hypothesis of electron energizing up to tens MeV in rather weak, but extended field near to the lightning leader [20]. Further development and numerical simulations are required to prove or reject this hypothesis. Very interesting model, in which REs acquire large energies from electromagnetic pulse generated by horizontal lightning discharge and penetrating to the upper stratosphere [17, 18], needs taking into account the self-consistent field. Besides the fractal approach Milikh and Valdivia implemented in the framework of the spherical approximation [18] needs more detailed substantiation because RE distributions in thunderstorm fields are strongly anisotropic [21].

Started with the pioneer work [7], a mechanism of the breakdown in the atmosphere in rather weak thundercloud field controlled by relativistic RE avalanches (RREAs) is being developed as alternate to the classical mechanism. The mechanism permits breakdown in fields with strength below the threshold required for the ordinary breakdown. Capability to account for in a unified manner both the high-altitude optical phenomena and TGFs and TNFs is the advantage of the mechanism. Basing on this mechanism a theory of UAD is being developed (cf. review [22]) and numerical simulations are being conducted (for instance, [23 – 34]). Variety of simulated thundercloud charge configurations and duration of lightning discharge triggering the breakdown leads to

[1)] e-mail: babich@elph.vniief.ru; kay@sar.ru

different RE space-time distributions. The variety is quite natural, as the observational data do not allow reliable selecting configurations, which could account both for high-altitude optical phenomena and for TGFs and TNFs, though the promoting in this direction is doubtless [35, 36]. Results of TGF calculations [13, 23 – 26, 29 – 31, 34] agree with the BETSI data [5, 37], in spite of that out-of-date and strongly overestimated RREA rates were used, except [13, 29, 30, 34]. Lehtinen et al. and Babich et al. allowed for the geomagnetic field [29], which is obvious advantage, especially in view of that the TGF majority was detected in the tropical zone [6]. However, too large values of the adopted cloud charge $Q = 1200\,\mathrm{C}$ and its size $\sim 100\,\mathrm{km}$ is obvious shortcoming of simulations by Lehtinen et al. [29]. Later Lehtinen et al. reduced the charge to $Q = 450\,\mathrm{C}$ located at the altitude $H = 15\,\mathrm{km}$ [30]. As in our earlier work [13], here we used more realistic Q and H, namely, 100 C and 10 km; 130 C and 14 km; 200 C and 14 km. Besides, the process of the electric field switching on above the cloud was simulated.

In the present paper, in difference to the recent papers [34, 35], characteristics of BETSI [5] and RHESSI [6] TGF are calculated basing on direct 2D numerical simulation of UAD driven by RREAs in self-consistent electric field. In difference to [12] the (γ, n)-yield in TNFs is computed consistently with UAD using the calculated source of hard bremsstrahlung responsible for the TGFs. Optical emissions are calculated with a goal to check the model adequacy by comparing with observed high-altitude fluorescence [38 – 40].

Discharge numerical model. The model is the further development of the 1.5D model used for simulating of the high altitude optical phenomena only and distinguished for the multi-group description of RE kinetics [32, 33] implemented, however, in the framework of RE current tube approximation with á priori set discharge radius. Here the multi-group technique is implemented in the framework of consistently 2D fluid approach. The motion of ions is taken into account. This is especially important in the vicinity of the disks (see below) modeling the cloud charges. The set responsible for the optical emissions is distinguished for detailed description of excitation with allowing for the vibrational kinetics permitting receiving accurate distribution of the light over separate lines.

The multigroup technique enables receiving RE energy distributions and accurate simulating of RE penetration to the space altitudes, which is important for correct calculating of γ-radiation transport to the satellite altitudes. The RE population is distributed over N energy groups in the range $[\varepsilon_{\mathrm{th}}, \varepsilon_{\max}]$, where $\varepsilon_{\mathrm{th}}$ is the runaway threshold (the second root of the equation $F(\varepsilon) = eE$ [41]) and $\varepsilon_{\max}$ is defined by an idiosyncrasy of a particular problem. The RE kinetics is described by a set of group equations [42] reduced from a full set, including continuity, energy balance and motion group equations [43]. Data on cosmic rays [44] were used to calculate the RE source. In difference with our earlier simulations [28 32, 33] up-to-date accurate dependence of RE multiplication time t_{run} on the "overvoltage" $\delta = eE/(F_{\min} \cdot P)$ [21] was used. Here eE is the electric force, $F_{\min} = 218\,\mathrm{keV/m{\cdot}atm.}$ is the minimal value of the drag force $F(\varepsilon)$ acting on RE with the energy ε due to interactions with molecules, P is the local pressure. Results for 10-group of REs are presented below.

Kinetics of secondary and background electrons of low energies and positive and negative ions was described in the framework of the drift approximation with allowing for the ionization by REs and electrons of low energies, electron-ion recombination and electron attachment to oxygen molecules. Literature data were used for dependencies of the kinetic coefficients on E/P. External (cosmic ray) sources of background electrons, negative and positive ions and REs were used.

The strength of selfconsistent electric field was calculated solving the current continuity equation [27, 32, 33].

The weakly ionized plasma between the cloud top and ionosphere initially shields the cloud field. As a lightning carries away the positive upper charge of the cloud, a field of negative polarizing charges near the top appears. The external field is modeled by that of uniformly charged thin disk located at the altitude H and reflected relative to the Earth surface ($z = 0\,\mathrm{km}$) and the lower electrosphere boundary ($z = 60\,\mathrm{km}$). The disk radius is calculated according to the formula

$$R_{\mathrm{disk}}(t) = \begin{cases} \sqrt{q(t)/2\pi\varepsilon_0 E_{\max}}, & t \le t_{\mathrm{disch}} \\ \sqrt{Q_{\max}/2\pi\varepsilon_0 E_{\max}}, & t \ge t_{\mathrm{disch}} \end{cases}, \qquad (1)$$

where $q(t) = Q_{\max} \cdot (t/t_{\mathrm{disch}})$ is the instantaneous value of the charge, $Q_{\max}$ is its maximum value, t_{disch} is the lightning discharge duration, $E_{\max}$ corresponds to $\delta_{\max} = eE_{\max}/F_{\min}P(z) = 7$ accepted at the disk surface. Two versions of switching on the field of the polarizing charges were simulated:

(1) variable disk radius R_{disk}, such that $\sigma_{\mathrm{disk}} = q(t)/\pi R^2_{\mathrm{disk}}(t) = \mathrm{const} = 2\varepsilon_0 \cdot E_{\max}$;

(2) $R_{\mathrm{disk}} = \mathrm{const}$, so that the charge density varied according to the formula $\sigma = q(t)/\pi R^2_{\mathrm{disk}}$.

The maximum charge density corresponds to $\delta = eE_{\max}/F_{\min}P(H) = 7$ at the disk surface.

Results of simulation of high-altitude optical phenomena. Space-time evolution of charged parti-

cle number densities and air fluorescence were obtained in the result of numerical simulation for $t_{\rm disch} = 1$ ms and realistic values of $Q_{\max}$ and H (100 C, 10 km; 130 C, 14 km; 200 C, 14 km). The air fluorescence into four main bands was calculated: the first positive system 1P ($\lambda = 570$–1040 nm, $B^3\Pi_g \to A^3\Sigma_u^+$ transitions of N_2), Meinel system M ($\lambda = 500$–2000 nm, $A^2\Pi \to X^2\Sigma$ transitions of N_2^+), the second positive 2P and first negative system 1N ($\lambda = 290$–530 nm, $C^3\Pi_u \to B^3\Pi_g$ transitions of N_2 and $B^2\Sigma_u \to X^2\Sigma_g^+$ of N_2^+).

Qualitatively results for optical phenomena are close to those given by 1.5D model [32, 33], however, the glow brightens is several times larger. Note that neither TGFs nor TNFs were not simulated in [32, 33]. Calculated brightness and color of the fluorescence, its space – time evolution agree with observational data of Blue Jets and Red Sprites [38, 40]. The fluorescence duration caused by RREAs is of ~ 1 ms. In agreement with indication of Taranenko and Roussel–Dupré [24] the very long duration of Blue Jets, namely, ~ 100 ms, was calculated to be a consequence of the fluorescence originating from the recombination of positive and negative ions after ceasing of RREAs generation.

The general agreement of the calculated characteristics of the optical emissions with observational data of high-altitude optical phenomena testifies both to the model adequacy and trustworthiness of the computed dependencies of RE number density on the spatial coordinates and time, required for calculating TGF and TNF characteristics.

For simulated configurations ($Q_{\max}$, $H = 100$ C, 10 km; 130 C, 14 km; 200 C, 14 km) and both versions of the field switching on the RE flux is mainly concentrated in the domain adjacent to the disk (thundercloud), i.e. in the Blue Jet domain.

In view of the characteristic time of TGFs is close to the duration of Red Sprites and much less than that of Blue Jets, Nemiroff et al. [37] connected the TGF origin with Red Sprites. However, the duration of the pulse of REs capable of emitting hard bremsstrahlung and concentrated mainly within the Blue Jet domain is of ~ 1 ms, whereas the prolonged Blue Jet fluorescence, ~ 100 ms, is the radiation of decaying plasma. Moreover, so few REs achieve the Red Sprite altitudes that the excitation of the air mainly by low-energy electrons stipulates the Red Sprite.

Hard gamma-ray generation. To interpret the TGFs a number of bremsstrahlung photons emitted by UAD into a solid angle $\Delta\Omega = S_{\rm det}(\xi/H_{\rm orbit})^2$ in the direction to the satellite and capable of achieving the orbit altitude $H_{\rm orbit}$ was calculated integrating over the Blue Jet domain where REs are concentrated:

$$N_\gamma^{(i)} = \frac{dN_\gamma}{dt} f_2(\bar\varepsilon_i, \bar\mu) \cdot \Delta\Omega \cdot \iint n_{\rm run})\mathbf{r}, t)P(z)\times$$
$$\times \Delta_i \cdot \exp\left(-\frac{l_{\rm opt}(z)}{\lambda_i}\right) \cdot dV\,dt. \qquad (2)$$

Here $n_{\rm run}(\mathbf{r}, t)$ is the RE concentration; dN_γ/dt is the rate of the bremsstrahlung generation at P = 1 atm. per one RE and $f_2(\bar\varepsilon_i, \bar\mu)$is the steady energy and angular photon distribution function [45]; $\bar\mu$ is the mean cosine of an angle between a direction of the photon propagation and the local electric force $-e\mathbf{E}$; $S_{\rm det}$ is the detector efficient area; i is a number of the energy channel of the detector of the radiation with mean energy $\bar\varepsilon_i$, Δ_i is a share of photons emitted into the channel i; $l_{\rm opt}(z) = (h_{\rm char}/\xi)\exp(-z/h_{\rm char})$ is the optical length of the air layer between the altitudes z where Blue Jet develops and the orbit altitude ($H_{\rm orbit} \gg z$); $h_{\rm char} = 7.1$ km is the exponential atmosphere characteristic scale; ξ is the cosine of an angle between a direction to the satellite and the vertical; $\lambda_i = \lambda(\bar\varepsilon_i)$ is the range of photon with the mean energy $\bar\varepsilon_i$ at P = 1 atm. [46].

Photon distributions over the energy channels [5] and total photon numbers N_γ calculated for smaller $\bar\mu$ and ξ are consistent with experimental data [5] processed by Nemiroff et al. [37]. The distribution calculated for $\bar\mu = \xi = 0.7$ especially well fits the panel displayed in fig.1j [37]. In the case $\bar\mu = \xi = 1$, which apparently accounts for the less probable configuration, the calculated N_γ almost two orders of the value exceeds the measured N_γ.

Calculated $n_{\rm run}(\mathbf{r}, t)$ were used to analyze the new measurements of TGFs aboard RHESSI [6]. The best agreement with [6] was obtained at small $\bar\mu$ and ξ: for $\bar\mu = \xi = 0.5$ in the case $Q_{\max} = 130$ C and $H = 14$ km and $\bar\mu = \xi = 0.5$ and 0.7 in the case $Q_{\max} = 200$ C and $H = 14$ km. Most likely, this result indicate that smaller $\bar\mu$ and ξ account better for the photon energy decrease due to cascade processes with the photon participation and better correspond to the satellite location with respect to TGF sources. The calculated photon energy distribution $dN_\gamma/d\varepsilon_\gamma$ for $Q_{\max} = 200$ C and $H = 14$ km is illustrated in figure.

The calculated mean photon energies $\bar\varepsilon_\gamma$ at RHESSI are presented in the table 1. At larger $Q_{\max}$ the γ-spectra at the satellite altitude are enriched by low-energy photons and correspondingly $\bar\varepsilon_\gamma$ is less. The reasons are obvious. In the case of larger $Q_{\max}$ REs penetrate to higher altitudes. The photons of lower energies, which dominate in the RE bremsstrahlung, generated at high altitudes experience weaker absorption along their way to the satellite than those produced in the dense layers and are capable to achieve the satellite. The lower $\bar\varepsilon_\gamma$ better fit the RHESSI data.

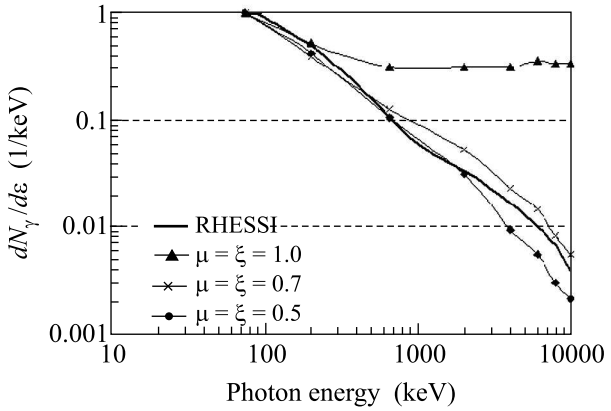

Comparison of computed γ-ray spectrum with RHESSI TGF-spectrum [6]. $Q_{\max} = 200\,\mathrm{C}$, $H = 14\,\mathrm{km}$

Table 1

Calculated mean photon energies $\bar{\varepsilon}_\gamma$ at RHESSI

$Q_{\max}$, H	130 C, 14 km	200 C, 14 km
Number of emitted photons per discharge ($\varepsilon_\gamma \geq 10\,\mathrm{keV}$)	$7.62 \cdot 10^{21}$	$9.93 \cdot 10^{21}$
$\bar{\mu} = \xi = 1$	9.5 MeV	8.0 MeV
$\bar{\mu} = \xi = 0.7$	4 MeV	2.1 MeV
$\bar{\mu} = \xi = 0.5$	3 MeV	1.27 MeV

Neutron generation. The consistency of the calculated γ-ray characteristics, especially for $Q_{\max} = 200\,\mathrm{C}$ and $H = 14\,\mathrm{km}$, with TGFs also testifies to the model adequacy. So the γ-ray characteristics in the source (Blue Jet) are reliable for calculating numbers of photonuclear neutrons from Blue Jet. The yield of photonuclear neutrons from UAD was calculated letting the neutrons to be generated along the photon range $\lambda_\gamma(z) = \lambda_\gamma(0)/P(z)$:

$$N_n = 2N_{\mathrm{L}}\lambda_\gamma(0)\frac{dN_\gamma}{dt}\iint n_\gamma(\mathbf{r},t)\times$$

$$\times P(z)\int\limits_{\varepsilon_{\mathrm{th}}(\gamma,n)}^{\varepsilon_{\gamma,\max}} f_\gamma(\delta,\varepsilon_\gamma)\sigma(\gamma,Sn)d\varepsilon_\gamma dV\,dt. \qquad (3)$$

Here $n_\gamma(\mathbf{r},t)$ is the photon number density ($n_\gamma(\mathbf{r},t) \approx \approx r_{\mathrm{run}}(\mathbf{r},t)$ [45]); N_{L} is the Loshmidt's number; $f_\gamma(\delta,\varepsilon_\gamma)$ is the photon distribution over energies ε_γ normalized per unit [45]; $\sigma(\gamma,Sn)$ is the total cross-section of (γ,n)-reactions [47]; $\varepsilon_{\mathrm{th}}(\gamma,1\mathrm{n})$ is the $(\gamma,1\mathrm{n})$-reaction threshold; $\varepsilon_{\gamma,\max}$ is a maximal energy, up to which data on the cross-sections are available. Within the accuracy of the present calculations it is sufficient to let the atmosphere to be consisted of the ^{14}N nuclei, for which $\varepsilon_{\mathrm{th}}(\gamma,1\mathrm{n}) = 10.55\,\mathrm{MeV}$ and $\varepsilon_{\gamma,\max} = 29.5\,\mathrm{NeV}$ [47]. In this energy range $\lambda_\gamma(0) \approx 500\,\mathrm{m}$ [46].

The results of calculations are presented in the table 2. The obtained values $N_n \sim 10^{14}-10^{15}$ are consistent with the analytical estimation $N_n \sim 10^{15}$ [12] carried out for the cloud charge $Q_{\mathrm{cloud}} = 210\,\mathrm{C}$ and $H = 18\,\mathrm{km}$ with allowing for the geomagnetic field, which apparently compensated the effect of lower air density than in the present simulations ($H = 14\,\mathrm{km}$).

Table 2

(γ,n) neutron yield per discharge

$Q_{\max}$, C	100	130	200
H, km	10	14	14
$N_n/10^{14}$	4.9	7.6	10.7

Conclusions. For three configurations of thundercloud charges within the framework of mechanism of breakdown controlled by RREAs numerical simulations of UAD and high-altitude optical phenomena were executed, results of which agree with field observations of Blue Jets and Red Sprites. The glow of the decaying secondary plasma accounts for the very long duration of Blue Jets, $\sim 100\,\mathrm{ms}$.

From the calculated RE space-time distributions the characteristics of RE bremsstrahlung were computed, which agree with numbers and spectra of TGF photons detected aboard BETSI [5,37] and RHESSI [6] spacecrafts. Simulations prove that TGFs originate from the Blue Jet domain, where the avalanche multiplication of REs takes its course and almost total RE flux is concentrated. This result is consistent Dwyer and Smith [34] and Williams et al [35] who, proceeding from results of rather simplified simulations, placed the TGF origin in the upper troposphere/lower stratosphere (15–21 km).

For the simulated configurations the photonuclear neutron numbers appeared to be rather large, of $\sim 10^{14}-10^{15}$, and match to the analytical estimation [12]. As shown in [12], it is too small to account for the TNFs detected in correlation with thunderstorm discharges at the Earth's surface [8–10]. Possibly the photonuclear neutrons were generated by lightning discharges, which occur much nearer to the ground. Proving that the TNFs are connected with atmospheric discharges would be a serious support of the mechanism of the breakdown in the atmosphere controlled by RREAs [7,22]. The predicted neutron numbers, $\sim 10^{14}-10^{15}$, are large enough to be measured by instruments aboard aircraft and spacecraft.

The authors use an opportunity to express their deepest gratitude to academician R.I. Il'kaev and Dr.

S.J. Gitomer for the support of the research in atmospheric electricity, to academician A.V. Gurevich, Dr. R.A. Roussel-Dupré, Dr. E.M. Symbalisty and RAS corresponding member K.P. Zybin for the long-term collaboration in this area.

1. C. T. R. Wilson, Proc. Cambridge Phil. Soc. **22**, 534 (1924).
2. A. S. Eddington, Nature **2948** (suppl.), 25 (1926).
3. G. E. Parks, B. H. Mauk, R. Spiger, and J. Chin, Geophys. Res. Lett. **8**, 1176 (1981).
4. M. MacCarthy and G. E. Parks, Geophys. Res. Lett. **12**, 393 (1985).
5. G. J. Fishman, P. N. Bhat, R. Mallozzi et al., Science **264**, 1313 (1994).
6. D. M. Smith, L. I. Lopez, R. P. Lin et al., Science **307**, 1085 (2005).
7. A. V. Gurevich, G. M. Milikh, and R. A. Roussel-Dupre, Phys. Lett. A. **165**, 463 (1992).
8. G. N. Shah, H. Razdan, G. L. Bhat et al., Nature **313**, 773 (1985).
9. A. N. Shyam and T. C. Kaushik, J. Geophys. Res. **104**, 6867 (1999).
10. B. M. Kujevskii, *Bulletin of the Moscow University*, Ser. 3, Physics. Astronomy, no 5, 2004, p. 14.
11. R. L. Fleisher, J. Geophys. Res. **80**, 5005 (1975).
12. L. P. Babich, JETP Letters **84**, 285 (2006).
13. L. P. Babich, R. I. Il'kayev, I. M. Kutsyk et al., Geomagnetism and Aeronomy **44**, 243 (2004).
14. V. P. Pasko, U. S. Inan, Y. N. Taranenko, and T. F. Bell., Geophys. Res. Lett. **22**, 365 (1995).
15. V. P. Pasko, U. S. Inan, and T. F. Bell., Geophys. Res. Lett. **23**, 301 (1996).
16. V. P. Pasko, U. S. Inan, T. F. Bell, and Y. N. Taranenko, J. Geophys. Res. **102**, 4529(1997).
17. Yu. P. Raizer, G. M. Milikh, M. N. Shneider, and S. V. Novakovski, J. Phys. D: Appl. Phys. **31**, 3255 (1998).
18. G. M. Milikh and J. A. Valdivia, Geophys. Res. Lett. **26**, 525 (1999).
19. N. Liu and V. P. Pasko, J. Geophys. Res. **109**, A04301 (2004).
20. G. D. Moss, V. P. Pasko, N. Liu, and G. Veronis, J. Geophys. Res. **111**, A02307, doi:10.1029/2005JA011350 (2006).
21. L. P. Babich, E. N. Donskoy, R. I. Il'kayev et al., Plasma Physics Reports **30**, 616 (2004).
22. A. V. Gurevich and K. P. Zybin, Phys. Usp. **44**, 1119 (2001).
23. N. G. Lehtinen, M. Walt, U. S. Inan et al., Geophys. Res. Lett. **23**, 2645, (1996).
24. Yu. N. Taranenko and R. A. Roussel-Duprè, Geophys. Res. Lett. **23**, 571 (1996).
25. N. G. Lehtinen, V. P. Pasko, and U. S. Inan, Geophys. Res. Lett. **24**, 2639 (1997).
26. N. G. Lehtinen., V. P. Pasko, and U. S. Inan, Geophys. Res. Lett. **24**, 2639 (1997).
27. V. Yukhimuk, R. A. Roussel-Duprè, E. M. D. Symbalisty et al., Geophys. Res. Lett. **25**, 3289 (1998).
28. I. M. Kutsyk and L. P. Babich, Phys. Lett. A **253**, 75 (1999).
29. N. G. Lehtinen, T. F. Bell, and U. S. Inan, J. Geophys. Res. **104**, 24699 (1999).
30. N. G. Lehtinen, U. S. Inan, and T. F. Bell, J. Geophys. Res. **106**, 28841 (2001).
31. R. A. Roussel-Dupre, E. Symbalisty, Y. Taranenko, and V. Yukhimuk, J. of Atmospheric and Solar-Terrestrial Phys. **60**, 917 (1998).
32. L. P. Babich, R. I. Il'kayev, I. M. Kutsyk et al., Doklady Earth Sciences **388**, 106 (2003).
33. L. P. Babich, R. I. Il'kayev, I. M. Kutsyk et al., Geomagnetism and Aeronomy **44**, 231 (2004).
34. J. R. Dwyer and D. M. Smith, Geophys. Res. Lett. **32**, L22804, doi: 1029/2005GL023848 (2005).
35. E. Williams, R. Boldi, J. Bór et al., J. Geophys. Res. 111, D16209, doi:10.1029/2006JD006447 (2006).
36. S. A. Cummer, Y. Zhai, W. Hu et al., Geophys. Res. Lett. **32**, L08811, doi:10.1029/2005GL022778 (2005).
37. R. J. Nemiroff, J. T. Bonnell, and J. P. Norris, J. Geophys. Res. **102**, 9659 (1997).
38. D. D. Sentman and E. M. Wescott, Phys. Plasmas **2**, 2514 (1995).
39. V. P. Pasko, M. Stenley, J. D. Mathews et al., Nature **416**, 152 (2002).
40. M. Fullekrug et al. (editors), *Sprites, Elves and Intense Lightning Discharges*, Springer, Netherlands, 2006.
41. L. P. Babich, High Temperature **33**, 190 (1995).
42. A. Yu. Kudryavtsev, Cand. Sc. (Ph. D.) theses, Lomonosov Moscow State University, 2005 [In Russian].
43. L. P. Babich and M. L. Kudryavtseva, JETP **128**, no 4 (2007), to be published.
44. R. R. Daniel and S. A. Stephens, Rev. of geophys. and space physics **12**, 233 (1974).
45. L. P. Babich, E. N. Donskoy, I. M. Kutsyk et al., Geomagnetism and Aeronomy **44**, 697 (2004).
46. D. P. Grechukhin, *Gamma-radiation*, in: Physical encyclopedia, Vol. 1, Ed. A.M. Prokhorov, Soviet encyclopedia edition, Moscow, 1988 [in Russian].
47. S. S. Dietrich and B. L. Berman, Atomic Data and Nucl. Tables **38**, 199 (1988).